Journal Name

ARTICLE TYPE

Cite this: DOI: 10.1039/xxxxxxxxxx

The nanostructure of a lithium glyme solvate ionic liquid at electrified interfaces†

Samuel W. Coles,[a] Maksim Mishin,[b,c], Susan Perkin*,[a], Maxim V. Fedorov*,[d,b] and Vladislav B. Ivaništšev*[c]

Received Date
Accepted Date

DOI: 10.1039/xxxxxxxxxx

www.rsc.org/journalname

Solvate ionic liquids are a subclass of ionic liquids that have the potential to be used in a range of electrochemical devices. We present molecular dynamics simulations of the interfacial structure of thin films of one such lithium based solvate ionic liquid, [Li(G4)][TFSI], an equimolar solution of tetraglyme and lithium bistriflimide. This solvate ionic liquid is shown to form a novel interfacial structure at a plane electrode, which differs in a number of ways from the nanostructure observed for a conventional ionic liquid at similar interfaces. This paper explores the structural composition of the interfacial layers of this solvate ionic liquid, including their variation with surface charge, and the relation between chemical structure and interfacial arrangement.

Introduction. The suitability of ionic liquids as electrolytes in electrochemical devices has been discussed frequently over the past decade.[1–6] Normally the ionic liquids proposed for these applications are aprotic ionic liquids consisting of a bulky organic cation paired with one of a variety of anions. Recently, a sub-class of ionic liquids, solvate ionic liquids, have begun to be viewed as another set of potential electrolyte candidates.[7–10] In these ionic liquids the traditional bulky organic cation is replaced with a long-lived complex consisting of an atomic metal cation bound to solvent. In most cases this complex consists of the metal cation and a single polydentate solvent molecule.[8] If every cation is bound to a solvent molecule then, at equimolar concentration (1:1 salt to solvent), the liquid consists solely of complex ions, with no free solvent, like a conventional ionic liquid[8]. However, in reality, all solvate ionic liquids contain a fraction of cations uncoordinated to solvent. The percentage of free ions (here defined as cations not coordinated to a solvent molecule) varies depending on the relative affinities of the solvent molecule and the anion for coordinating to the metal ion: when binding of cation to solvent is substantially more favourable than cation–anion coordination then the large majority of cations in the liquid will be coordinated to solvent. Liquids that meet these conditions are described as "good solvate ionic liquids"; these liquids exhibit behaviours close to conventional ionic liquids.[11] When a substantial fraction of anions bind to cations in place of cation–solvent associations, and so a larger percentage of solvent molecules remain uncoordinated, the system behaves more like a concentrated solution. These liquids are described as "poor solvate ionic liquids".[11]

A well-studied class of solvate ionic liquids consists of an equimolar mixture of an organic lithium salt and a glyme. Glymes are a family of short chain methoxy terminated oligoethers, the general structure of which is shown in panel A of Fig. 1. The homologous series of glymes adopts the naming convention $H_3C(O–C_2H_4)_n–OCH_3 \equiv Gn$; the G4 oligoether employed in this work is also referred to as tetraglyme. One solvate ionic liquid

[a] Department of Chemistry, University of Oxford, South Parks Road, Oxford OX1 3QZ, United Kingdom; E-mail: susan.perkin@chem.ox.ac.uk
[b] Department of Physics, Scottish Universities Physics Alliance (SUPA), Strathclyde University, John Anderson Building, 107 Rottenrow East, Glasgow G4 0NG, United Kingdom.
[c] Institute of Chemistry, University of Tartu, Ravila 14a, Tartu 50411, Estonia; E-mail:vladislav.ivanistsev@ut.ee
[d] Skolkovo Institute of Science and Technology, Skolkovo Innovation Center, Moscow 143026 Russia; E-mail:m.fedorov@skoltech.ru

† Electronic Supplementary Information (ESI) available:Containing a discription of the nanosturcutre at the positive electrode, simmulations of bulk solvate ionic liquid, Cell potential plots, and Force Field parameters. See DOI: 10.1039/b000000x/

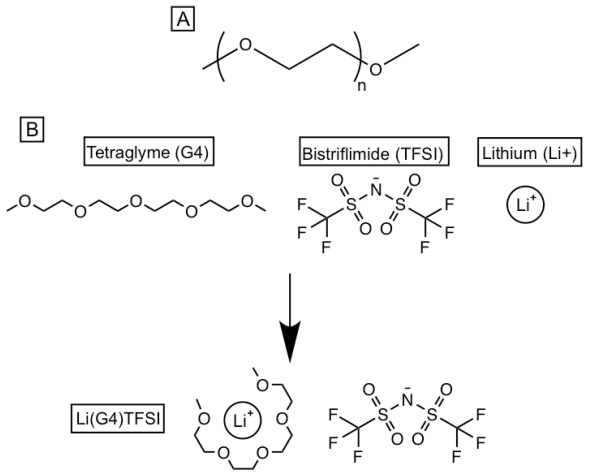

Fig. 1 Panel A shows the general structural formula of glymes, a glyme consisting of n ethoxy repeat units termed G_n and therefore contains $(n+1)$ oxygen atoms. Panel B shows the formation of [Li(G4)][TFSI] from the constituent salt and glyme.

formed from tetraglyme is [Li(G4)][TFSI], an equimolar mixture of tetraglyme (G4) and lithium bistriflimide as shown in Panel B of Fig. 1. [Li(G4)][TFSI] can be considered as the archetypal good solvate ionic liquid: previous studies showed this liquid to have only ca. 2.4% of glyme molecules unchelated to metal ions.[11] Electrochemical and NMR analysis showed the diffusion constants of glyme molecules and lithium ions to be equivalent, a sign of a large percentage of ions being coordinated.[11,12] Additionally, a thermogravimetric analysis showed this liquid to have a single thermal decomposition point, at a temperature much higher than pure solvent, as opposed to a slow burning off of solvent seen with poor solvate ionic liquids where a sizeable amount of the solvent is free[11].

Three major studies on the topic of the bulk nanostructure of solvate ionic liquids were performed by Murphy *et al.*[13], Shimazu *et al.*[14], and Saito *et al.*[15] These three studies suggested somewhat different lithium–glyme oxygen coordination environments, with the work of Murphy *et al.* showing a much lower lithium to glyme oxygen coordination number (2.27) than in the other studies. The most recent study by Saito *et al.* suggested a structure where the three central glyme oxygen atoms are coordinated to lithium over a longer timescale than the outer oxygens which dynamically coordinate and uncoordinate. Saito *et al.* reported a vastly different coordination number to Murphy *et al.* (4.4). Further to this molecular dynamics simulations, producing a variety of lithium glyme oxygen coordination numbers have been successfully used to interpret experimental results. Across all reported simulations coordination numbers ranging from 3.2 to 4.5[14–17] are reported (for temperatures between 297 K and 300 K). This work utilises the force field developed by Shimizu *et al.* which produces a coordination number roughly at the centre of this range[14]. Further computational studies of [Li(G4)][TFSI] and similar compounds include *ab initio* calculations for the complex cation[15,18–21] and density functional theory to study the interaction between the complex cation and highly oriented pyrolytic graphite (HOPG)[22].

The nanostructure of [Li(G4)][TFSI] at interfaces was studied experimentally using atomic force microscopy by McLean *et al.*[22] Their work showed diversity in the interfacial nanostructures adopted by [Li(G4)][TFSI], with variation in the structure dependent on both electrode potential and electrode material. For instance for positive potentials extended layering analogous to that seen in conventional ionic liquids is observed. However, at gold electrodes at the same potential a different nanostructure, with fewer layers at the interface of lower thickness, appears to arise.

Here we present molecular dynamics simulations of solvate ionic liquids at interfaces. The specific system studied consists of [Li(G4)][TFSI] (an equimolar mixture LiTFSI and tetraglyme) at a graphene-like slab of Lennard–Jones Particles with non zero charge. The results obtained provide context and insight to experimental results obtained by McLean *et al.* and provide deeper understanding of the more complex and nuanced interfacial structure of solvate ionic liquids as compared to standard aprotic ionic liquids. We find these liquids have a novel nanostructure at the negative electrode (modeled as a surface with a given negative charge density), compared to conventional ionic liquids. Further to this, we find that many lithium cations in the first interfacial layers are coordinated to more than one glyme molecule contrary to the simplified portrait in Fig.1.

Methodology. Molecular dynamics simulations of solvate ionic liquids were performed using Gromacs 5.1 package.[23–29] The simulation setup is similar to the setups used in previous work studying conventional aprotic ionic liquids.[30–33]. The system consists of two periodic electrodes of dimensions 6.8160 nm by 6.8866 nm separated by 12.1000 nm.

Force fields were identical to previous simulations of the bulk nanostructure of this solvate ionic liquid performed by Shimizu *et al.*[14]. The OPLS-AA force field is used for the glyme,[34] while the (OPLS-AA-derived) CL&P force field is utilised for the simulations of the ionic components of the electrolyte.[35] . This force field was first used to study the bulk nanostructure[14] , it was shown to reproduce the structure factor observed in experimental x-ray defraction data. Further to this, the number of uncoordinated lithium ions and glyme molecules is also found to be markedly similar to NMR results obtained by Ueno et al.[36]. The simulations also reproduced the experimental trends in transport prop-

erties across a range of solvate ionic liquids, though as with most non polariseable ionic liquid force fields[37] the transport properties observed are not quantatively comparable with experimental data[14].

The electrode is modelled as an array of Lennard–Jones spheres in a hexagonal structure with lattice structure similar to that of graphene, with a charge spread evenly across every atom in the electrode. Moreover, positions of the electrode atoms were fixed for the duration of the simulation. The gap between the electrodes is filled with 964 ion pairs, and 964 glyme molecules.

The initial orientations of ions within the simulation box are generated using the packmol algorithm[38]. Initial energy minimisation is performed by use of the steepest descent algorithm. After this, the system is annealed from a temperature of 350 K to a temperature of around 800 K and back to 350 K over the course of 5 ns (consisting of 5×10^6 steps of 1 fs). The system is further equilibrated at 350 K for 0.5 ns (consisting of 5×10^5 steps of 1 fs). The system that is generated from this phase is used as the starting point for the centre of mass pulling steps described later. This system is also used as the starting point for a 2 ns production run at 350 K (consisting of 2×10^6 steps of 1 fs). This process is repeated to produce three replicas. Simmulations are run at 350 K as opposed to ambient conditions in order to decrease viscocity and therefore increase sampling, an approach that has been use in studies of conventional ionic liquids[31] . This approach is further justified by the realtive similarity in lithium coordination environment in bulk solution at 300 K and 350 K presented in the supplementary information.

Centre of mass pulling (COM Pulling) is employed to generate a number of replicas with a lithium probe particle varying distances away from the surface of the electrode, as in previous work looking at alkali metal ionic liquid solutions[32,39]. Unlike in previous simulations, in this work, there is no predefined probe prior to COM pulling. Instead, a lithium ion that is located near to the surface of the electrode at the end of the equilibration phase is assigned as the probe. This probe ion is then manually shifted to a distance of 0.1 nm from the electrode. The probe is then pulled at constant speed over the course of 3.5 ns to generate a set of systems with separations between the plane of the electrode and the probe ranging from 0.1 nm to 4.8 nm in steps of 0.05 nm. Each of these systems undergoes a 1 ns production run with the probe frozen in place. The average forces acting on the probes during these production runs are used to calculate a potential of mean force for the lithium ion approaching the electrode by pulling. This process is performed for two lithium ions in each initial replica leading to 6 replicas for each charge and each lithium probe location.

The simulations described were performed under NVT conditions, with temperature conditions maintained using the V-rescale thermostat.[23–25,29] The Coulomb and van der Waals cut-offs were set to 1 nm. Long-range electrostatics were performed using the particle mesh Ewald method, with a slab geometry[40,41].

Results and Discussion.

Nanostructure at Negatively Charged Surfaces. Fig.2 shows density distribution functions for lithium cations, bistifilimide nitrogen anions, and the central oxygen of each glyme molecule for the solvate ionic liquid [Li(G4)][TFSI] in the region adjacent to a surface. Panels b–d show the varying density distributions as surface charge varies from $0\,\mu C/cm^2$ to $-10\,\mu C/cm^2$. The density of each of the atoms shown shows substantial deviation from bulk density in the 1–2 nm region away from the electrode surface indicating clear interface-induced structuring. Of particular note, the peaks corresponding to lithium cations and glyme central oxygen atoms remain at closely similar positions throughout the range of surface charge studied. In contrast, the peaks arising from the anion nitrogen atom shift substantially in response to the changing surface charge. The density of glyme in the layer closest to the electrode (peak at ca. 0.3 nm) increases dramatically as the electrode becomes more negative, and this can be understood as counterbalancing the complete loss of anion density in the near-surface region at negative surface charges. On the other hand, the density of lithium cations alters only marginally as the electrode is negatively charged. Put together, these observations leads to a picture of co-ion expulsion from the near-surface region, rather than counterion adsorption, as a mechanism of electrode screening.

The distinction between co-ion expulsion and counterion adsorption is useful principally in systems where solvent is present to 'fill the gaps'; in a pure ionic liquid the two come hand-in-hand because – to a large extent – the expulsion of a co-ion requires concomitant adsorption of a counterion, (i.e. ion exchange), to maintain total density. The balance between these mechanisms, and their relative importance as solvent is introduced into ionic liquids, has been analysed and discussed recently[42,43]. Simulations showing how, for a standard ionic liquid, increasing surface charge leads to counter-ions staying at the electrode surface and co-ions move a little further from the surface have also been reported.[33,44–46] Further increasing charge leads to the formation of a charged multilayer where a distinct layer of co-ions forms behind the first layer of counter-ions. At even higher charges the charged monolayer and crowded structures are observed in simulations[33].

Here, in contrast, the presence of glyme molecules leads to a different behaviour: in [Li(G4)][TFSI] the multilayer type structure is not observed even at a relatively high surface charge. As the surface charge becomes increasingly negative, and negative ions are expelled from the interfacial region, glyme molecules take the place of anions, and the concentration of cations is maintained relatively constant. This implies a variation in the ratio of cations to glyme molecules in the interfacial region, away from

the 1:1 bulk value. This implies that glyme molecules are performing a role of free solvent as well as ligand for the lithium cations in the near-surface region. A later section will look at another key implication of Fig. 2 that lithium cations do not move into direct contact with the electrode.

The nanostructure at positively charged surfaces is less distinctively different to the structure observed in aprotic ionic liquid mixtures, for example see refs[30,44,47,48], our simulations of these interfaces are provided in the supplementary information.

Coordination environment of lithium ions at the negative electrode. We now turn to the coordination environment of lithium ions in the near surface region. In the previous section it was noted that an excess of glyme exists in the region closest to a negative electrode surface. This leads to a greatly increased chance of a lithium cation being coordinated to two glyme molecules. This is explored in Fig.3 which shows the coordination numbers of lithium ions to each of two different glyme molecules. In Fig.3 each heat map shows the relative probability that a lithium ion in the near-surface region (the area within 1nm of the the interface) will be coordinated with n oxygen atoms from one glyme molecule and m oxygen atoms from a second glyme molecule. In the case where $n = 0$ or $m = 0$, the lithium is only coordinated to one glyme molecule.

Examining Fig.3 one can see that, at zero surface charge, a noteable fraction of lithium ions are not coordinated to any glyme molecules (i.e. $m = 0$ and $n = 0$). This is due to the presence, at zero surface charge, of negative bistriflamide ions which may coordinate the lithium in place of glyme. As the charge of the surface becomes more negative, no "free" lithium ions are observed and all are coordinated to glymes: this occurs due to bistriflimide ion depletion from the surface layer and replacement with glyme molecules.

There are two main lithium coordination environments observed in Fig.3: (i) coordination to five oxygen atoms all from one glyme molecule (i.e. $m = 5$ and $n = 0$ or *vice versa*), and (ii) coordination to two glyme molecules *via* three coordinating oxygen atoms on each. The increasingly glyme-rich environment brought about by increasing negative surface charge promotes coordination to multiple glyme molecules, i.e. type (ii) is seen to a greater extent at higher negative surface charge.

It is interesting to note this the preference for either 5-coordinate complexes with a single ligand or 6-coordinate complexes with two tri-dentate ligands. We propose that this effect is due to lithium cations preference for coordination to six oxygen atoms. The 5-coordnate glyme complex is favoured when the glyme concentration is equal to lithium concentration and anions are present, allowing for the lithium to coordinate to 5 oxygens in the coordinating glyme molecule, and a single bistriflimide anion. The complex consisting of the two tri-dentate glyme ligands occurs at higher surface charges due to depletion of anions and increase in glyme concentration. In this environment Lithium cations will coordinate to the two glyme molecules in order to obtain a coordination number of six. This data is not inconsitent with the previously reported semihelical dimer[49,50] and extended helical chains[51] observed in previous studies of the bulk nanostructure of other lithium glyme systems. In general the coordination structure observed in the present simmulations is more disordered than that observed in earlier studies. Inspection of the number of lithium cations coordinated to each glyme molcule shows that in this case glyme molecules appear to coordinate to a single lithium cation, with under 5 percent of glyme molecules coordinating to more than one lithium cation across all interfacial charges.

These findings suggest that at the negative electrode, solvate ionic liquids do not coordinate solely in a one-to-one manner (as is predominant in the bulk) and so the interfacial structure is distinctly and qualtiatively different to the bulk. It is likely this diversity in the environment will have an effect on the properties of this solvate ionic liquid at charged interfaces. In particular reactivity and electrochemical stability of this complex ion would be affected. In turn, these effects could have implications for charge transfer in electrochemical devices employing this electrolyte and therefore the macroscopic electrochemical stability and device efficiency.

Lithium ion behaviour at the negative electrode. We now discuss the observation (from Fig.2) that lithium cations remain at a fixed distance from the electrode when the electrode charge is varied; lithium cations do not appear to move into direct contact with the electrode in this system at any studied surface charge. To investigate this interesting finding further, we studied the potential of mean force for a lithium cation approaching a negative or uncharged electrode; the results are shown in Fig 4. The shape of the plots shows that coordination of lithium cations to the electrodes is unfavourable. Lithium cations are increasingly stabilised closer to electrode at increasing surface charge. However, this effect is more than counteracted by decreasing the minimum in the mean force potential, observed at the higher charges. This leads to the depletion of the already small number of lithium ions closer than 0.4 nm from the electrode at a surface charge of $-5\,\mu\mathrm{C/cm^2}$ (Fig.2). One possible mechanism for the low lithium–electrode coordination is that it is more favourable for lithium cations to maximise their coordination number with glyme molecules. This would cause a layer of glyme oxygens to be closer to the electrode than lithium cations are, exactly as observed in Fig.2.

Further inspection of the potential of mean force in Fig. 4 shows minima occurring every 0.4 nm after a slightly more complicated structure in the first interfacial layer, the same periodicity of lithium ion peaks observed in Fig.2. Experimental studies with an Au(111) surface by McLean *et al.* appears to correlate with this structure, at a surface potential of 0.5 V layers of 0.4 nm are

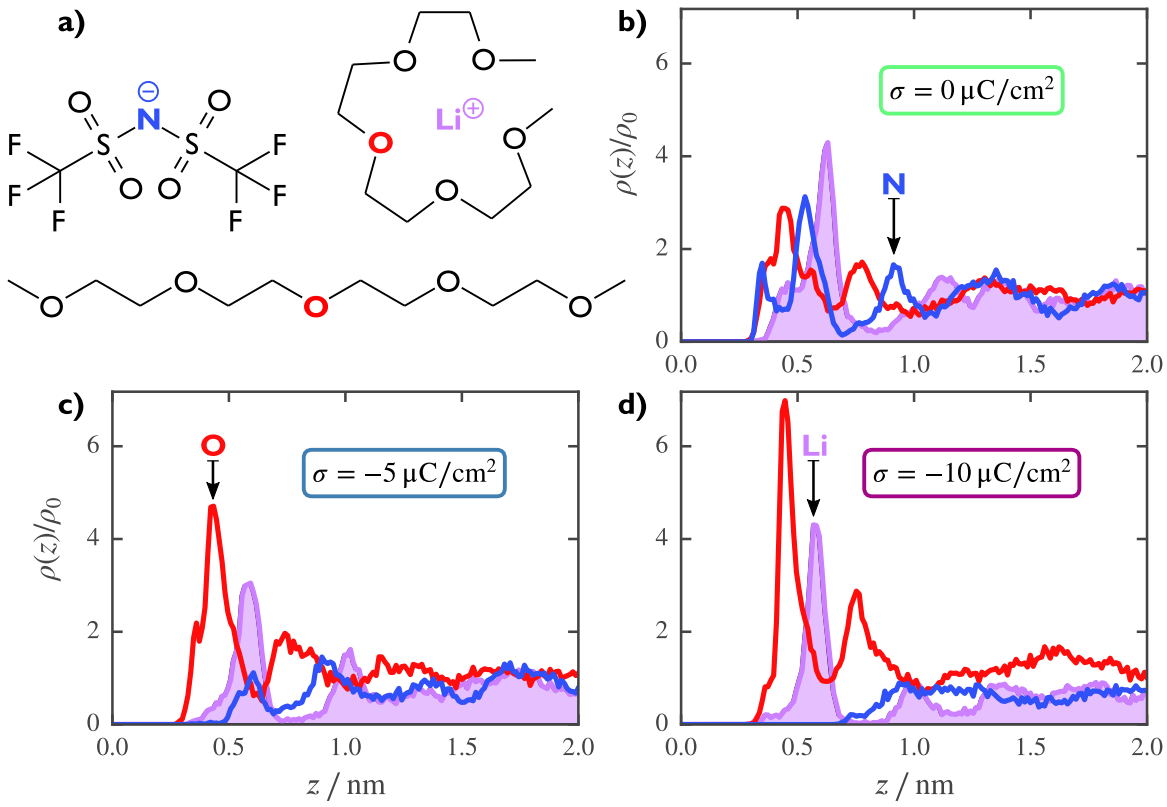

Fig. 2 Structural formula of bistriflimide anion, lithium–glyme complex cation and tetraglyme with colored atoms to indicate the colour code in subsequent panels (a), and relative number density profiles ($\rho(z)/\rho_0$) of bistriflimide nitrogen (blue), Li^+ (purple), and central glyme oxygen (red) (b–d). The model electrode with surface charge values of $0\,\mu C/cm^2$ (b), $-5\,\mu C/cm^2$ (c), and $-10\,\mu C/cm^2$ (d) is situated at $z = 0$ nm.

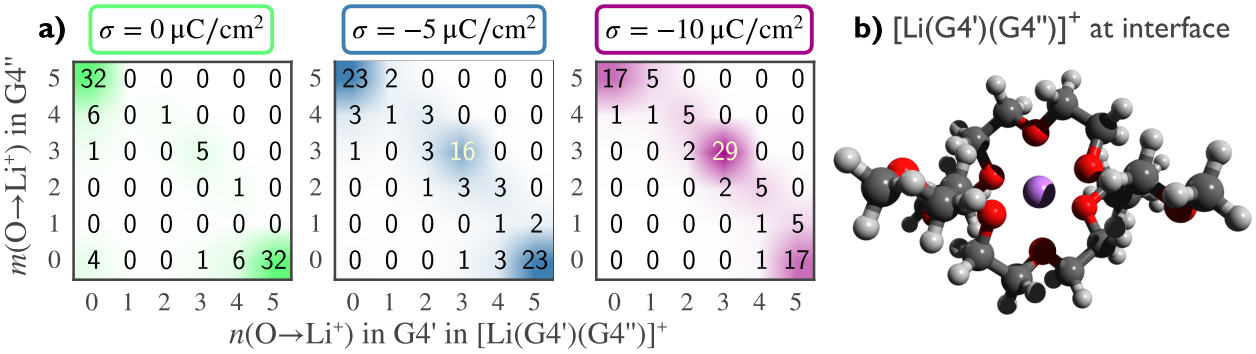

Fig. 3 Integer Percentage of Li^+ coordinated by n oxygens from G4' and m oxygens from G4" in the first layer of interface with surface charge values of $0\,\mu C/cm^2$, $-5\,\mu C/cm^2$ and $-10\,\mu C/cm^2$ (a). A CPK model of [Li(G4')(G4")] with $n = 3$ and $m = 3$ found at lower surface charges (b). The sum of integers in each diagram is less than 100 due to rounding down of a large number of elements with small values close to zero.

observed.[22] after a thicker initial layer. These layers appear to be made up of both cations, mostly coordinated to glyme molecules, and anions leading to this smaller layer thickness than would be observed in a multilayer interfacial structure.

Conclusion. In conclusion, lithium glymes adopt a distinct nanostructure at the negative electrode unlike that observed in

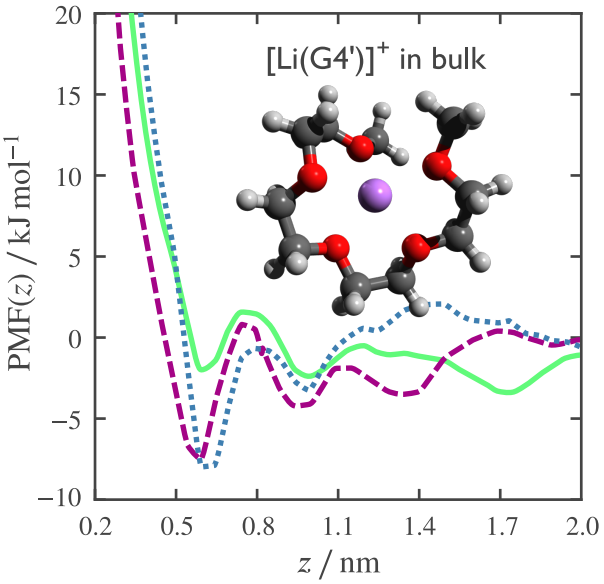

Fig. 4 Potential of mean force profiles (PMF(z)) for Li^+ approaching the surface with surface charge values of $0\,\mu C/cm^2$ (light green solid line), $-5\,\mu C/cm^2$ (blue dotted line) and $-10\,\mu C/cm^2$ (dark violet dashed line). The inset shows a CPK model of lithium–glyme complex ion with a coordination number of 5 which is typical for bulk [Li(G4)][TFSI].

conventional ionic liquids. This structure is brought about by the repulsion of bistriflimide anions and the enrichment of neutral glyme molecules in their place when the electrode is negatively charged. Strongly favourable coordination of the lithium by the glyme ligands prevents large scale desolvation of the lithium as required for the lithium to approach close to the electrode; instead the lithium remains separated from the electrode by a distance determined by the width of a glyme molecule. These factors together lead to lithium cations in the area closest to the negative electrode being coordinated to more than one glyme molecule, quite different to the 1:1 lithium ion–glyme structure favoured in the bulk of the liquid. The disruption of this bulk 1:1 coordination and the excess of glyme present in the near-electrode region raises two questions: whether [Li(G4)][TFSI] actually is a good solvate ionic liquid in the area closest to the negative electrode and what effect does this have on the electrochemical properties of the liquid?

Acknowledgements

The presented simulations results were obtained using the EPSRC funded ARCHIE-WeSt High Performance Computer (www.archie-west.ac.uk). EPSRC grant no. EP/K000586/1. SWC thanks EPSRC and the Department of Physical and Theoretical Chemistry at the University of Oxford for his DTA studentship. This research was supported the Estonian Personal Research Project PUT1107 and by the EU through the European Regional Development Fund (Centre of Excellence, 2014-2020.4.01.15-0011). This research was also supported by a short term scientific mission funded by COST action MP1303. SP is supported by The Leverhulme Trust (RPG-2015-328) and the ERC (under Grant Agreement 676861: LIQUISWITCH).

References

1 F. Béguin, V. Presser, A. Balducci and E. Frackowiak, *Adv. Mater.*, 2014, **26**, 2219–2251.
2 D. R. MacFarlane, N. Tachikawa, M. Forsyth, J. M. Pringle, P. C. Howlett, G. D. Elliott, J. H. Davis, M. Watanabe, P. Simon and C. A. Angell, *Energy Environ. Sci.*, 2014, **7**, 232–250.
3 M. V. Fedorov and A. A. Kornyshev, *Chem. Rev.*, 2014, **114**, 2978–3036.
4 H. Liu, Y. Liu and J. Li, *Phys. Chem. Chem. Phys.*, 2010, **12**, 1685–1697.
5 M. Armand, F. Endres, D. R. MacFarlane, H. Ohno and B. Scrosati, *Nat. Mater.*, 2009, **8**, 621–629.
6 A. Lewandowski and A. Świderska-Mocek, *J. Power Sources*, 2009, **194**, 601–609.
7 K. Takechi, Y. Kato and Y. Hase, *Adv. Mater.*, 2015, **27**, 2501–2506.
8 T. Mandai, K. Yoshida, K. Ueno, K. Dokko and M. Watanabe, *Phys. Chem. Chem. Phys.*, 2014, **16**, 8761–8772.
9 K. Ueno, *J. Electrochem. Soc. Jp.*, 2016, **84**, 674–680.
10 R. Tatara, N. Tachikawa, H.-M. Kwon, K. Ueno, K. Dokko and M. Watanabe, *Chem. Lett.*, 2013, **42**, 1053–1055.
11 K. Ueno, K. Yoshida, M. Tsuchiya, N. Tachikawa, K. Dokko and M. Watanabe, *J. Phys. Chem. B*, 2012, **116**, 11323–11331.
12 C. Zhang, K. Ueno, A. Yamazaki, K. Yoshida, H. Moon, T. Mandai, Y. Umebayashi, K. Dokko and M. Watanabe, *J. Phys. Chem. B*, 2014, **118**, 5144–5153.
13 T. Murphy, S. K. Callear, N. Yepuri, K. Shimizu, M. Watanabe, J. N. Canongia Lopes, T. Darwish, G. G. Warr and R. Atkin, *Phys. Chem. Chem. Phys.*, 2016, **18**, 17224–17236.
14 K. Shimizu, A. A. Freitas, R. Atkin, G. G. Warr, P. A. FitzGerald, H. Doi, S. Saito, K. Ueno, Y. Umebayashi, M. Watanabe and J. N. Canongia Lopes, *Phys. Chem. Chem. Phys.*, 2015, **17**, 22321–22335.
15 S. Saito, H. Watanabe, Y. Hayashi, M. Matsugami, S. Tsuzuki, S. Seki, J. N. Canongia Lopes, R. Atkin, K. Ueno, K. Dokko, M. Watanabe, Y. Kameda and Y. Umebayashi, *J. Phys. Chem. Lett.*, 2016, 2832–2837.
16 D. J. Eyckens, B. Demir, T. R. Walsh, T. Welton and L. C. Henderson, *Phys. Chem. Chem. Phys.*, 2016, **18**, 13153–13157.
17 S. Tsuzuki, W. Shinoda, M. Matsugami, Y. Umebayashi, K. Ueno, T. Mandai, S. Seki, K. Dokko and M. Watanabe, *Phys. Chem. Chem. Phys.*, 2015, **17**, 126–129.
18 S. Terada, T. Mandai, S. Suzuki, S. Tsuzuki, K. Watanabe, Y. Kamei, K. Ueno, K. Dokko and M. Watanabe, *J. Phys. Chem. C*, 2016, **120**, 1353–1365.
19 T. Mandai, K. Yoshida, S. Tsuzuki, R. Nozawa, H. Masu, K. Ueno, K. Dokko and M. Watanabe, *J. Phys. Chem. B*, 2015, **119**, 1523–1534.
20 K. Yoshida, M. Nakamura, Y. Kazue, N. Tachikawa, S. Tsuzuki, S. Seki, K. Dokko and M. Watanabe, *J. Am. Chem. Soc.*, 2011, **133**, 13121–13129.
21 S. Tsuzuki, W. Shinoda, S. Seki, Y. Umebayashi, K. Yoshida, K. Dokko and M. Watanabe, *ChemPhysChem*, 2013, **14**, 1993–2001.
22 B. McLean, H. Li, R. Stefanovic, R. J. Wood, G. B. Webber, K. Ueno, M. Watanabe, G. G. Warr, A. Page and R. Atkin, *Phys. Chem. Chem. Phys.*, 2015, **17**, 325–333.
23 S. Páll, M. J. Abraham, C. Kutzner, B. Hess and E. Lindahl, *Solving Software Challenges for Exascale*, Springer International Publishing, Cham, 2015, vol. 8759, pp. 3–27.
24 M. J. Abraham, T. Murtola, R. Schulz, S. Páll, J. C. Smith, B. Hess and E. Lindahl, *SoftwareX*, 2015, **1-2**, 19–25.
25 S. Pronk, S. Páll, R. Schulz, P. Larsson, P. Bjelkmar, R. Apostolov, M. R. Shirts, J. C. Smith, P. M. Kasson, D. v. d. Spoel, B. Hess and E. Lindahl, *Bioinformatics*, 2013, **29**, 845–854.
26 B. Hess, C. Kutzner, D. van der Spoel and E. Lindahl, *J. Chem. Theory Comput.*, 2008, **4**, 435–447.
27 S. Páll and B. Hess, *Comput. Phys. Comm.*, 2013, **184**, 2641–2650.
28 D. van der Spoel, E. Lindahl, B. Hess, G. Groenhof, A. E. Mark and H. J. C. Berendsen, *J. Comput. Chem.*, 2005, **26**, 1701–1718.
29 H. J. C. Berendsen, D. van der Spoel and R. van Drunen, *Comput. Phys. Comm.*, 1995, **91**, 43–56.
30 M. V. Fedorov and R. M. Lynden-Bell, *Phys. Chem. Chem. Phys.*, 2012, **14**, 2552–

2556.
31 R. M. Lynden-Bell, A. I. Frolov and M. V. Fedorov, *Phys. Chem. Chem. Phys.*, 2012, **14**, 2693–2701.
32 V. Ivaništšev, T. Mendez-Morales, R. M. Lynden-Bell, O. Cabeza, L. J. Gallego, L. M. Varela and M. V. Fedorov, *Phys. Chem. Chem. Phys.*, 2016, **18**, 1302–1310.
33 V. Ivaništšev, M. V. Fedorov and R. M. Lynden-Bell, *J. Phys. Chem. C*, 2014, **118**, 5841–5847.
34 W. L. Jorgensen, D. S. Maxwell and J. Tirado-Rives, *J. Am. Chem. Soc.*, 1996, **118**, 11225–11236.
35 J. N. Canongia Lopes and A. A. H. Pádua, *J. Phys. Chem. B*, 2004, **108**, 16893–16898.
36 K. Ueno, R. Tatara, S. Tsuzuki, S. Saito, H. Doi, K. Yoshida, T. Mandai, M. Matsugami, Y. Umebayashi, K. Dokko and M. Watanabe, *Phys. Chem. Chem. Phys.*, 2015, **17**, 8248–8257.
37 V. Chaban, *Phys. Chem. Chem. Phys.*, 2011, **13**, 16055–16062.
38 L. Martínez, R. Andrade, E. G. Birgin and J. M. Martínez, *J. Comput. Chem.*, 2009, **30**, 2157–2164.
39 V. Gómez-González, B. Docampo-Álvarez, T. Méndez-Morales, O. Cabeza, V. B. Ivaništšev, M. V. Fedorov, L. J. Gallego and L. M. Varela, *Phys. Chem. Chem. Phys.*, 2017, **19**, 846–853.
40 U. Essmann, L. Perera, M. L. Berkowitz, T. Darden, H. Lee and L. G. Pedersen, *J. Chem. Phys.*, 1995, **103**, 8577–8593.
41 I.-C. Yeh and M. L. Berkowitz, *J. Chem. Phys.*, 1999, **111**, 3155–3162.
42 R. Burt, K. Breitsprecher, B. Daffos, P.-L. Taberna, P. Simon, G. Birkett, X. S. Zhao, C. Holm and M. Salanne, *J. Phys. Chem. Lett.*, 2016, **7**, 4015–4021.
43 A. A. Lee and S. Perkin, *J. Phys. Chem. Lett.*, 2016, 2753–2757.
44 V. Ivaništšev, S. O'Connor and M. V. Fedorov, *Electrochem. Commun.*, 2014, **48**, 61–64.
45 S. Xu, S. Xing, S.-S. Pei, V. Ivaništšev, R. Lynden-Bell and S. Baldelli, *J. Phys. Chem. C*, 2015, **119**, 26009–26019.
46 M. Z. Bazant, B. D. Storey and A. A. Kornyshev, *Phys. Rev. Lett.*, 2011, **106**, 046102.
47 A. I. Frolov, K. Kirchner, T. Kirchner and M. V. Fedorov, *Faraday Discuss.*, 2012, **154**, 235–247.
48 A. S. Pensado, F. Malberg, M. F. C. Gomes, A. A. H. Pádua, J. Fernández and B. Kirchner, *Phys. Chem. Chem. Phys.*, 2014, **4**, 18017–18024.
49 P. Jankowski, M. Dranka, G. Z. Żukowska and J. Zachara, *J. Phys. Chem. C*, 2015, **119**, 9108–9116.
50 W. A. Henderson, N. R. Brooks and V. G. Young, *Chem. Mater.*, 2003, **15**, 4685–4690.
51 Z. Gadjourova, D. Martín y Marero, K. H. Andersen, Y. G. Andreev and P. G. Bruce, *Chem. Mater.*, 2001, **13**, 1282–1285.